Tundra uptake of atmospheric elemental mercury drives Arctic mercury pollution

Authors: Daniel Obrist[1,2*], Yannick Agnan[2,3], Martin Jiskra[4], Christine Hedge[2], Dominique Colegrove[5], Jacques Hueber[5], Christopher Moore[2,6], Jeroen Sonke[4], Detlev Helmig[5]

Affiliations:

[1]Department of Environmental, Earth, and Atmospheric Sciences, University of Massachusetts, Lowell, MA 01854, USA

[2]Division of Atmospheric Sciences, Desert Research Institute, 2215 Raggio Parkway, Reno, Nevada 89512, USA.

[3]Milieux Environnementaux, Transferts et Interactions dans les hydrosystèmes et les Sols (METIS), UMR 7619, Sorbonne Universités UPMC-CNRS-EPHE, 4 place Jussieu, F-75252 Paris, France.

[4]Geosciences Environnement Toulouse, CNRS/OMP/Université de Toulouse, 14 Avenue Edouard Belin, 31400 Toulouse, France.

[5]Institute of Arctic and Alpine Research (INSTAAR), University of Colorado, 4001 Discovery Drive, Boulder, Colorado 80309, USA.

[6]Gas Technology Institute (GTI), 1700 S Mount Prospect Road, Des Plaines, Illinois 60018, USA.

*Corresponding Author: E-mail: Daniel_obrist@uml.edu

Anthropogenic activities have led to largescale mercury (Hg) contamination in the Arctic[1-3] so that Hg tissue levels in modern-day wildlife including falcon and eagle feathers, polar bear hairs, and beluga whale teeth, are enhanced up to 10-fold[4-6]. High Arctic Hg contamination has been attributed to unique sea-salt-induced chemical cycling of Hg, termed Atmospheric Mercury Depletion Events (AMDEs), but their impacts are now debated[2,7] and are largely unknown away from the coast. Furthermore, wet deposition measurements in the Arctic show some of the lowest Hg deposition via precipitation worldwide[8] raising questions as to the sources of high Arctic Hg exposure. Based on the most comprehensive Hg deposition mass balance study so far, here we show that the main source of Hg (71%) in the interior Arctic tundra is derived from gaseous elemental Hg (Hg^0) deposition, rather than deposition via precipitation or AMDEs – which are both minor. Deposition of Hg^0, the form ubiquitously present in the global atmosphere, occurs throughout the year, including the Arctic winter, and is enhanced in summer by vegetation Hg^0 uptake. The tundra uptake of gaseous Hg^0 leads to high soil Hg concentrations and mass exceeding levels in temperate soils several-fold. Concurrent Hg stable isotope measurements in the atmosphere, snowpack, vegetation, and soils support that Hg^0 dominates as a source to the tundra, and we hence for the first time provide a fully independent confirmation of Hg isotope source tracing. Stable isotope data from an inland to coastal transect show high soil Hg consistently derived from Hg^0, suggesting that the Arctic tundra forms a globally-important Hg sink storing up to half the world's soil Hg. High tundra soil Hg also explains why rivers annually transport massive amounts of Hg (50–80 Mg y^{-1}) to the Arctic Ocean[9-11]. Hg stable isotope signatures now also suggest that Hg^0 may dominate as sources in mid-latitude ecosystems[12-15], and we hence call for a focus on monitoring strategies for Hg^0 deposition worldwide.

Hg pollution impacts are increasingly controlled by climate-change induced disturbances in aquatic and terrestrial biogeochemistry[16], with potentially the most significant consequences in the Arctic where warming occurs at a rate almost double the worldwide average[17,18]. Regulatory frameworks such as the recent UNEP Minamata Convention – aimed to reduce Hg contamination globally[19] – rely on understanding of Hg sources, which is currently lacking in the Arctic. The widespread Hg contamination observed across the Arctic is inconsistent with extremely low atmospheric wet deposition, which in Arctic ecosystems is found to be among the lowest globally.

For example, annual wet deposition of 2.1±0.7 μg m^{-2} yr^{-1} at Gates of the Arctic National Park in Alaska (Supplemental Table S1) is almost five times lower than wet deposition measured across 99 lower-latitude U.S. locations (9.7±3.9 μg m^{-2} yr^{-1})[8]. Also unclear are the origins of vast amounts of Hg that are annually transferred by Arctic rivers to the Arctic Ocean[9]. These riverine Hg inputs to the Arctic Ocean, which exceed direct atmospheric deposition[10,11], stand in contrast to predictions that rank Arctic catchments lowest in terms of watershed Hg storage globally[20]. Another potential Hg source, deposition due to sea-salt-induced AMDEs in springtime[21], long was thought to be responsible for high Arctic Hg deposition. However, AMDEs may cause much smaller net Hg deposition because most of the deposited Hg can revolatilize to the atmosphere before snow melts and studies provide inconclusive evidence about their importance for Arctic deposition[2,7].

Unlike wet deposition and deposition related to AMDEs, both of which are composed of oxidized Hg (Hg^{II}), deposition of gaseous elemental Hg^0 – the form which is subject to long-range atmospheric transport and global atmospheric distribution – is largely unconstrained and not measured by deposition networks. We recently reviewed 132 studies on gaseous Hg^0 exchange between the atmosphere and terrestrial surfaces and estimated net global terrestrial Hg^0 exchange to exhibit a wide range and large uncertainty, from a net deposition of 500 Mg yr^{-1} to a net emission (i.e., volatilization from ecosystems to the atmosphere) of 1650 Mg yr^{-1} [22]. The large uncertainty stems from an almost complete lack of whole-ecosystem Hg^0 exchange measurements among these studies.

Here we performed a mass balance of atmospheric Hg deposition in the Arctic tundra – a biome covering ~6% of the global land surface area – to determine the major Hg sources in one of the most remote ecosystems worldwide. We conducted a two-year field measurement campaign to constrain atmospheric Hg deposition at Toolik Field station on the North Slope of Alaska, USA, 200 km inland from the coast representing the interior tundra. We measured net gaseous Hg^0 exchange at the ecosystem-level using micrometeorological techniques, wet and dry Hg^{II} deposition, and vegetation Hg inputs from aboveground biomass. We correspondingly measured Hg stable isotopic signatures in the atmosphere, snowpack, vegetation, and soil, and quantified total mass of Hg sequestered in tundra snowpack, plants, and soils. We further measured

atmosphere-snow-soil Hg^0 gas concentration profiles to independently verify Hg^0 flux exchange and locate zones of atmospheric Hg^0 sources and sinks.

Gaseous Hg^0 was the dominant form of deposition (6.5±0.7 μg m^{-2} yr^{-1}) accounting for 71% of total deposition (Fig. 1). Wet Hg^{II} deposition amounted to less than 5% of Hg^0 deposition (Supplemental Table S2; 0.2±0.1 μg m^{-2} yr^{-1}) and even lower than previous low measurements from another Arctic site in Alaska[8]. Atmospheric Hg^{II} concentrations were below the detection limit (33 pg m^{-3}) during most of the measured period with the exception of March and early April during AMDEs when concentrations reached nearly 0.5 ng m^{-3} (Extended Data). We constrained atmospheric Hg^{II} dry deposition to 2.5 μg m^{-2} yr^{-1} (range 0.8 to 2.8 μg m^{-2} yr^{-1}) based on periodic measurements of atmospheric Hg^{II} concentrations (Supplemental Information). We observed temporarily elevated snow Hg levels during AMDEs, although the deposited Hg revolatilized to the atmosphere within days (Supplementary Information).

The dominance of gaseous Hg^0 deposition as a source to this ecosystem was independently confirmed by Hg stable isotope analyses. We comprehensively characterized Hg stable isotope composition of atmospheric Hg^0, snowfall and snowpack, vegetation, organic and mineral soil horizons, and bedrock samples. As observed in previous studies[12-15,23,24], atmospheric Hg^0 and Hg^{II}, bedrock Hg^{II}, and Hg^{II} deposited through AMDEs have unique $\delta^{202}Hg$, $\Delta^{199}Hg$, and $\Delta^{200}Hg$ signatures (Fig. 2 and Extended Data). We then quantified relative contributions of different Hg sources to vegetation and soil samples using endmember mixing models and triple isotopic signatures. Results show that atmospheric gaseous Hg^0 is the dominant source of Hg in vegetation (median: 90%), organic soils (73%), and upper mineral soils (55%). Hg^{II} deposition accounted for 10% to 22% of Hg in the two soil compartments; and residual Hg^{II} from AMDEs, transferred to the tundra soils after snowmelt, accounted for 0–5%. Geogenic Hg contributed in a range of 0% in organic soil horizons to ~40% in mineral soil horizons. These results confirm direct flux measurements demonstrating that gaseous Hg^0 deposition is the dominant source of mercury to the tundra at Toolik Field station. We measured soil Hg stable isotope signatures in three additional tundra sites along a transect from Toolik Field station to the Arctic Ocean (Fig. 2D) and considered values from an additional peat profile from Barrow, AK at the coast[24], and found no significant differences in isotope signatures between these soils and soils at Toolik Field station. We hence observed no higher contributions of AMDEs (maximum 5%) even in soils closer to the coast, and

show evidence that the source of Hg in tundra soils is consistently and predominantly derived from atmospheric Hg^0 uptake.

Continuous flux measurements allowed determination of temporal patterns of Hg^0 deposition. Gaseous Hg^0 deposition persisted throughout periods of snow cover (Fig. 1), with the exception of March and April when net emission of Hg^0 to the atmosphere was observed after AMDEs. From October through mid-May, Hg^0 deposition averaged 0.4±0.4 ng m^{-2} h^{-1} and accounted for 37% of total annual Hg^0 deposition. Gaseous Hg^0 concentration profiles in snow and soil air, measured with complementary trace gas systems (see Methods), confirmed that wintertime Hg^0 deposition occurred (Fig. 3). Snow pore air Hg^0 concentrations were consistently below atmospheric concentrations, and concentrations decreased further from the upper to lower snowpack such that concentrations at the soil-snow interface were less than 50% of atmospheric levels. Since diffusive and advective trace gas fluxes are a function of respective concentration gradients, these Hg^0 concentration profiles were consistent with a net atmospheric deposition flux of gaseous Hg^0 to the tundra ecosystem, providing a third means of verifying atmospheric Hg^0 deposition. Further analysis showed that the wintertime Hg^0 deposition was driven by a sink below the Arctic snowpack, most likely in the tundra soil (Supplementary Information). Such a soil Hg^0 sink has been observed in a temperate soil, but the mechanism for soil Hg^0 uptake remains unclear[25].

During snow-free periods from mid-May through September, Hg^0 deposition increased (rate of 1.4±1.0 ng m^{-2} h^{-1}) and continued to greatly exceed deposition of all other forms of Hg combined (78% of total summertime deposition). In fact, some of the strongest Hg^0 deposition occurred after the spring onset of the tundra vegetation growing season, indicating that tundra vegetation amplified gaseous Hg^0 deposition. Clearly identifiable by its Hg isotope signature (Fig. 2), Hg in aboveground vegetation was indeed primarily (90%) derived from atmospheric Hg^0 uptake as shown previously[12,14]. We calculated substantial Hg mass contained in aboveground vegetation (29 µg m^{-2}; Table S4) which can subsequently be transferred to tundra soils via plant senescence and litterfall.

The dominant and time-extended atmospheric deposition of gaseous Hg^0 to the Arctic tundra has implications for local, regional, and global Hg cycling. Deposition of globally ubiquitous gaseous Hg^0 leads to unexpectedly high Hg levels in these remote tundra soils. Based on ^{14}C age dating

that shows that soils at Toolik Field station are older than 7,300 years (Table S5), deposition of atmospheric Hg^0 and accumulation of Hg in soils must have occurred over millennia. Soil Hg concentrations in the active layer above the permafrost averaged 138±15 μg kg^{-1} in organic soil layers and 97±13 μg kg^{-1} in mineral soil horizons (Table S5), exceeding the 20–50 μg kg^{-1} range observed across temperate and tropical soils several-fold[26-28]. Riverine studies suggest that significant contributions by upland soil sources in the Arctic are needed in order to explain high Hg loadings[9,10]. The high tundra soil Hg levels, derived from Hg^0 uptake, hence explain the conundrum that watersheds with some of the lowest Hg wet deposition loads on Earth and limited impacts from AMDEs show elevated Hg in rivers and widespread Hg impacts on Arctic wildlife[3-6].

At the global scale, the Arctic tundra serves as an important repository for atmospheric Hg^0 emitted at mid-latitudes. Stable isotope analysis across four different tundra soils on the North Slope of Alaska confirm that atmospheric Hg^0 dominates as a source and suggests a large-scale Hg^0 sink across the Arctic tundra. Although few soil tundra Hg concentrations are reported elsewhere, our measurements along a 200 km northern Alaska transect and a few published data also show high soil Hg concentrations (Table S6). If a soil Hg pool of 27 mg m^{-2} at Toolik Field station (Table S5; top 40 cm) is representative of the global tundra belt, Arctic tundra soils would contain ~143 Gg of Hg, which would account for almost half the total estimated global soil Hg pool size of 300 Gg based on temperate studies for this soil depth[20,29]. Further, our study provides the first independent experimental verification of source attribution by Hg isotope signatures, which at this tundra site show that Hg stored in vegetation and soils is predominantly derived from atmospheric Hg^0 consistent with direct deposition measurements. Recent Hg stable isotope studies have suggested that gaseous Hg^0 deposition may dominate as a source in remote forests of the mid-latitudes[12-15] as well. We hence call upon regulators and the scientific community to reorganize deposition monitoring[30] to include deposition of Hg^0 which we expect to dominate as a source across remote ecosystems worldwide.

Methods:

The study site is located near Toolik Field station (68°38'N, 149°36'W), a research station operated by the University of Alaska, Fairbanks. All measurement systems were located in a tussock tundra with underlying soil types characterized as Typic Aquiturbels with active layer depths between 60 and 100 cm. All analyzers and control systems were housed in a temperature-controlled field laboratory (Extended Data Fig. E1) built on the tundra, and sampling lines and sensors were routed outside to the tundra sampling locations via heated conduits. This setup allowed year-round measurements of trace gas dynamics including through the Arctic winter without damage from icing, animal disturbances, or other issues.

Overview of key measurements: During two full years, we measured continuous net surface-atmosphere fluxes of gaseous Hg^0 (i.e., the balance of deposition and volatilization), that to our knowledge was conducted year-round previously only in two temperate grassland sites[31,32]. Campaign-style wet deposition measurements composed of Hg^{II} species[33] were conducted approximately every six weeks throughout the two years and included snowfall and rain measurements, surface snow and full snowpack collection, and subsequent analysis of total dissolved Hg after melting. Hg^{II} dry deposition was assessed by pyrolyzer measurements (see below) to quantify atmospheric Hg^{II} concentrations multiplied by deposition velocity. Hg^{II} dry deposition measurements were conducted only from January through September 2016, but we used auxiliary Arctic studies to constrain mid-winter patterns[1, 34] (see below and Extended Data). In addition, we measured gaseous Hg^0 in interstitial air of snowpack and tundra soils at multiple locations and depths in the tundra during two full years to assess atmosphere-snow-soil diffusion profiles and pinpoint active source and sink zones. For this, a snow tower (Fig. E1D;[35,36]) was deployed to measure Hg^0 gas concentrations in interstitial snow pores at multiple depths in the undisturbed tundra snowpack. In addition, a soil trace-gas system (Fig. E1E[37]) consisting of six gas wells provided gaseous Hg^0 concentrations in soil pores at three depths each in two tundra soil profiles. During summers, field campaigns were conducted for detailed characterization of concentrations and pool sizes of Hg in all major ecosystem matrices, including vegetation as well as organic and mineral soil layers. Characterization of Hg stable isotope compositions were conducted in snow, soils, plants, and the atmosphere to complement source and sink processes of Hg in this tundra ecosystem.

Micrometeorological flux measurements to quantify gaseous Hg^0 exchange at the ecosystem level were conducted using an aerodynamic flux method (Fig. E1C). Surface-atmosphere flux was calculated by measurement of concentration gradients in the atmosphere above the tundra in conjunction with atmospheric turbulence parameters as follows:

$$F_{Hg^0} = -\frac{k * u_* * z}{\phi_h(z/L)} * \frac{\partial c(Hg^0)}{\partial z} \quad (1)$$

where k denotes the von Karman constant (0.4), u_* the friction velocity, z the measurement height, $\phi_h(z/L)$ the universal temperature profile, L the Monin-Obukhov length, and $\partial c(Hg^0)/\partial z$ the vertical Hg^0 gas concentration gradient. Hg^0 concentrations at heights of 61 cm and 363 cm above the soil surface were measured through 0.2 µm Teflon® inlet filters connected to perfluoroalkoxy (PFA) lines, a setup that measures gaseous Hg^0 [37]. A valve control system with three-way solenoid valves (NResearch, West Caldwell, NJ, USA) allowed switching between the gradient inlets every 10 min. Solenoids were connected to a set of trace gas analyzers with a total sampling flow of 1.5 L min^{-1}. This system included an air mercury analyzer (Model 2537A, Tekran Inc. Toronto, Canada); a Cavity Ring-Down (CRD) greenhouse gas analyzer to measure CO_2, H_2O, and CH_4 (Los Gatos Research, San Jose, USA); an O_3 analyzer (Model 49C, Thermo Scientific, Waltham, USA); and an O_2 analyzer (Model 1440, Servomex, East Sussex, United Kingdom).

Fluxes were calculated only during periods of appropriate turbulence according to Edwards et al.[38] and periods when $z/L < -0.2$ and $z/L > 0.2$ were removed from the data set. The tundra measurement site was bordered by Toolik Lake to the north, and we removed data when flux footprints originated from Toolik Lake or it's edge (0-40° and 300-360°, 27% of the data). For gap filling of periods when measurements were missing, or when fluxes originated from the nearby lake, or when conditions did not fulfill the criteria for acceptable turbulence to calculate fluxes, we interpolated flux data using the average diel pattern of each respective month. For quality control, sampling lines were confirmed to be free of contamination during each field visit (approximately every six weeks using Hg-free air; Model 1100, Tekran Inc.). In addition, line inter-comparisons were conducted at the same interval to test for line biases between the upper and lower inlet lines; for this, both upper and lower inlet lines were set at the same height and measurements were conducted to assess offset. Line intercomparison tests showed no significant line offsets

228 throughout the study with the exception of one time when a leak was detected and immediately
229 fixed, and fluxes prior to that time were corrected.

230 ***A snow tower*** (Fig. E1D) to measure gaseous Hg^0 and auxiliary trace gas concentrations in the
231 undisturbed snowpack at multiple heights was deployed next to the flux tower (approximately 2
232 m distant). The snow tower, described in Seok et al.[35] and Faïn et al.[36], consists of vertical square
233 aluminum bars with 60 cm cross arms at five heights that hold a total of 10 sampling inlets.
234 Horizontal crossbars that support air inlets were set at heights of 0, 10, 20, 30, and 110 cm above
235 the soil surface, with the lower four inlets generally buried in snow most of winter to measure
236 snow pore air; the uppermost inlet always was located above the snowpack and measured
237 atmospheric Hg^0 gas concentrations. Each crossbar supported a pair of connected air inlets, spaced
238 60 cm apart, and fitted with 25 mm syringe filters with 1 µm glass fiber membranes (Pall Life
239 Sciences, Ann Arbor, Michigan, USA) connected to PFA lines. Snow tower lines were connected
240 to a Teflon valve control box and data acquisition system inside the heated laboratory. These lines
241 were connected to a second set of trace gas analyzers, including for gaseous Hg^0, ozone (same
242 models as above), as well as a CO_2 and H_2O analyzer (Model LI840A, LI-COR Inc., Lincoln,
243 USA). Sampling flow rates were set between 2.7 and 3.0 L min^{-1}, and the sampling sequence was
244 set to extract snow air at each height for 10-min measurement periods so that a full sequence of all
245 five inlet heights was sampled every 50 min. Measurements of ambient air gaseous Hg^0
246 concentrations measured at the top inlet of the snow tower system compared well to ambient air
247 Hg^0 concentrations measured by the micrometeorological tower.

248 ***A soil trace gas measurement system*** (Fig. E1E), similar to a system described in Obrist et al.[25],
249 was deployed to allow monitoring of soil pore trace gases at multiple depths and locations. In the
250 first year, the soil trace gas system consisted of six Teflon wells (63.5 cm length, 10.2 cm diameter)
251 with inside volumes of 4.2 L. One side of each well was perforated with 65 holes of 0.64 cm
252 diameter for a total perforated area of 20.6 cm^2. The holes were covered with Gore-Tex®
253 membranes and Teflon screens, both of which were held in place by stainless steel brackets and
254 pipe clamps for a watertight seal, allowing gas diffusion into the wells while keeping out soil water.
255 The soil wells were placed at two tundra soil profiles (10 cm, 20 cm, and 40 cm depths); one profile
256 consisted mainly of organic soil layers and a second mainly of mineral horizons. The six wells
257 were connected by PFA lines to the heated laboratory and connected to the same set of

instrumentation to measure trace gas gradients for flux measurements (gaseous Hg^0, CO_2, H_2O, CH_4, O_3, and O_2). The system, operated at a flow rate of 1.5 l min^{-1}, was programmed to extract a sequence of soil measurements (10 min. each) only three times per day to reduce the air volume extracted from the soil profile and minimize disturbance and advection effects. Because of water intrusion into the soil gas wells in June 2015, the system was replaced with a different system consisting of 47 mm Teflon inlet filters with additional inlet holes drilled at the bottom of the filters and mounted upside down in the soil profile at the same six locations. Testing in saturated water showed that the hydrophobic Teflon filters prevented water intrusion into the sampling lines using this inlet configuration. Both soil trace gas systems were extensively tested in Hg-free air and ambient air prior to deployment to confirm that they were free of contamination. These systems showed quick equilibrium with ambient air Hg^0 concentrations, and there was no memory effect when switching the sampling lines. Both measurement systems provided the same magnitude and seasonal patterns of gaseous Hg^0 soil concentrations (Fig. 3).

Atmospheric Hg^{II} concentrations were measured using a third gaseous mercury analyzer (Model 2537; Tekran Inc.) in conjunction with a pyrolyzer unit. Hg^{II} concentrations were calculated by differential measurements of air drawn from an inlet configured to measure gaseous Hg^0 (using 0.2 µm Teflon inlet filters) and a second inlet stream without a filter routed through a pyrolyzer oven set at 650º C, whereby all atmospheric Hg forms were converted into gaseous Hg^0 (i.e., measure total Hg). A valve switching unit (Model 1110, Tekran Inc.) was used to alternate measurements between total Hg and gaseous Hg^0 measurements every 10 min, and allowed calculating Hg^{II} concentrations by difference (similar to Lyman and Jaffe[39]). As a pyrolyzer oven, we modified a particulate mercury speciation module (Model 1135; Tekran Inc., Toronto, Canada) and used a quartz tube filled with quartz chips as pyrolyzer inlet that directly reached the ambient atmosphere for sampling. In addition, the particulate filter inside the glassware was removed, and the quartz tube was filled with quartz chips to increase the surface area and serve as an efficient catalyst. The detection limit of this system, based on three times standard deviation of the blanks, was 33 pg m^{-3}. The pyrolyzer unit was deployed from January through September 2016. Atmospheric Hg^{II} concentration measurements were lacking from October through mid-February, but we found undetectable (<0.033 ng m^{-3}) or low concentrations (generally <0.05 ng m^{-3}) in other winter months, similar to low or undetectable Hg^{II} concentrations outside of periods of AMDEs at

other Arctic locations[34]. For 2015, we assumed similar Hg^{II} concentrations as measured in 2016. Negative numbers in the Hg^{II} record represent noise levels of differential measurements as well as data are produced during strong fluctuations of total atmospheric Hg concentrations (i.e., during AMDE depletion recoveries). Atmospheric deposition of Hg^{II} was calculated to be 2.5 μg m^{-2} yr^{-1} based on multiplication of measured Hg^{II} concentrations with a proposed deposition velocity for Hg^{II} of 1.5 cm s^{-1} over various surfaces[40], with a range from 0.8 to 2.8 μg m^{-2} yr^{-1} (based on deposition velocities generally between 0.5 and 1.7 cm s^{-1})[41]. Even lower annual atmospheric Hg^{II} deposition has been independently estimated for this area based on nearby Arctic lake studies (0.1 μg m^{-2})[1]. Low wintertime Hg^{II} concentrations and deposition are further consistent with extremely low wintertime snowfall Hg concentrations (on average 0.26 ng L^{-1}; Supplementary Information Table S2) – which are derived from Hg^{II} scavenged from the atmosphere. Finally, stable Hg isotopic signatures were consistent with low amounts of Hg^{II} deposition measured at this site.

Atmospheric wet deposition of Hg (mainly Hg^{II} forms) and snow Hg^{II} was characterized by frequent collection of surface snow and manual collection of rainfall using trace-metal collection techniques (gloves, acid-cleaned Teflon and stainless steel sampling equipment). Samples were analyzed for Hg concentrations after filtration with 0.45 μm pore size filters. A total of 19 sampling dates were used for calculation of wet deposition loads (Table S2). Surface snow samples (top 3 cm) were directly transferred into new, sterile polyethylene sampling bags (Whirl-Pak®; Nasco, Fort Atkinson, WI, USA). Fresh snow was directly taken from the surface into the sampling bags; additional snowpack sampling was performed from the top to the bottom of the snowpack using acid-cleaned stainless steel cutters (Model RIP 1 1000 cc cutter; Snowmetrics, Fort Collins, CO, USA). In addition, snowpack sampling was performed on five dates using two excavated snow pits each that were sampled using stainless steel snow cutter (RIP 1 cutter 1000 cc) and then directly transferred to the sterile polyethylene sampling bags (double bags). Each snow pit was sampled at 10 cm-layer increments from the top to the bottom of the snow pit. Per layer, two replicate samples from perpendicular walls of the pit were each pooled together for analysis. Summertime collection of rainwater was performed manually using an acid-cleaned Teflon funnel and Teflon bottles. Determination of total dissolved Hg was performed according to U.S. EPA Method 1631 for total mercury in water using dual stage gold pre-concentration and an Hg water analyzer (Model 2600; Tekran Inc., Toronto, Canada). Annual atmospheric wet deposition was

calculated using volumetric precipitation measured at Toolik Field Station multiplied by respective snow and rain Hg concentrations (Table S2). Hg_{tot} and Hg_{diss} concentrations were determined using Tekran 2600 cold-vapor atomic fluorescence spectrometry (Tekran Instruments Corporation, Toronto, ON, Canada) using a bromine monochloride (BrCl) and hydroxylamine hydrochloride digestion following the EPA method 1631. The detection limits, determined as 3-times the standard deviation of blank samples, averaged 0.08 ng L^{-1}. Recoveries as determined by 5 ng L^{-1} standards analyzed after every 10 samples averaged between 93 and 107%. Laboratory and field blanks were conducted both for the stainless-stell cutter (using water rinses) and the whirl-pak bags used for snow sampling, and both showed no metal contamination (all blank determinations below detection limits).

Soil and vegetation Hg concentrations were determined from samples collected during multiple field sampling campaigns in spring through fall 2014, 2015, and 2016. All samples were freeze-dried, milled, and analyzed according to U.S. EPA method 7473 using a total mercury analyzer (Model MA-2000; Nippon Inc., Takatsuki, Japan) and as described in detail in Obrist et al.[26]. To estimate annual Hg uptake by vegetation and standing aboveground biomass pools (Table S4), data on vegetation dynamics (aboveground net primary productivity: NPP; and aboveground vegetation biomass) were used from Shaver and Chapin[41] and Chapin et al.[42].

Hg Stable isotope measurements were performed on Hg extracted from subsamples of dried and milled vegetation, soil, and rock samples using a two-step oven combustion system[14]. Snow samples were processed using a purge and trap system described by Sherman et al.[23] which was scaled up to 20 L bottles to attain Hg amounts large enough from low-concentrated snow samples. Sample blanks, recoveries, and Hg isotopic composition of processing standards (NIST-3133) were analyzed (Table E4). Atmospheric gaseous Hg^0 was collected continuously from a separate inlet at the flux tower, equipped with a glass fiber filter (as described for snow tower measurements) and a heated PFA line to the field laboratory. Atmospheric gaseous Hg^0 (typically sampled at 0.2 lpm for periods of 6–8 weeks) was collected on iodated activated carbon traps (IC-traps, 125 mg) which were processed with a combustion method adapted from Fu et al.[43]. Gaseous Hg^0 breakthrough of IC-traps was measured regularly during the sampling campaign using a Tekran 2537 mercury analyzer and was always below the detection limit (0.05 ng m^{-3}). Procedural blanks, procedural standards, and sample recoveries were measured for quality assurance (Table

E1). Hg isotopic ratios were measured by cold vapor – multi-collector inductively coupled plasma mass spectrometry (CV-MC-ICPMS; Neptune, Thermo-Finnigan, Germany) at the Midi-Pyrenees Observatory (Toulouse, France) applying measurement protocols described elsewhere[13,43].

Hg isotopic signatures are expressed using common nomenclature of small delta notation for mass-dependent signatures (MDF):

$$\delta^{xxx}Hg_{NIST-3133} = \left(\frac{(^{xxx}Hg/^{198}Hg)_{Sample}}{(^{xxx}Hg/^{198}Hg)_{NIST-3133}} - 1\right) \times 10^3 \quad (2)$$

where xxx corresponds to masses 199, 200, 201, 202, and 204. Mass-independent Hg isotopic signatures (MIF) are expressed by capital delta notation:

$$\Delta^{yyy}Hg = \delta^{yyy}Hg - (\delta^{202}Hg \times sf) \quad (3)$$

where yyy corresponds to the mass of 199, 200, 201, and 204 and *sf* to the kinetic mass-dependent scaling factors of 0.2520, 0.5024, 0.7520, and 1.493 for Δ^{199}Hg, Δ^{200}Hg, Δ^{201}Hg, and Δ^{204}Hg, respectively. Analytical precision and accuracy were assured through repetitive measurements of in-house standards ETH-Fluka (δ^{202}Hg = -1.43±0.19‰, Δ^{199}Hg 0.08±0.07‰, Δ^{200}Hg 0.02±0.07‰, 2SD, n=38) and UM-Almaden (δ^{202}Hg = -0.56±0.10‰, Δ^{199}Hg -0.02±0.06‰, Δ^{200}Hg 0.01±0.07‰, 2SD, n=9) which were in agreement with previously reported values[12-14].

References:

1. Fitzgerald, W. F. *et al.* Modern and historic atmospheric mercury fluxes in northern Alaska: global sources and Arctic depletion. *Environ. Sci. Technol.* **39**, 557-568 (2005).
2. Douglas, T.A. *et al.* The fate of mercury in Arctic terrestrial and aquatic ecosystems, a review. *Environ. Chem.* **9**, 321 (2012).
3. AMAP, "AMAP Assessment 2011: Mercury in the Arctic. Arctic Monitoring and Assessment Programme (AMAP)" (Oslo, Norway, 2011).
4. Dietz, R. *et al.* Time trends of mercury in feathers of West Greenland birds of prey during 1851-2003. *Environ. Sci. Techn*. **40**, 5911 (2006).
5. Dietz, R. *et al.* Trend in mercury in hair of Greenlandic polar bears (Ursus maritiumus) during 1892-2001. *Environ. Sci. Techn*. **40**, 1120 (2006).
6. Outridge, P.M. *et al*. A comparison of modern and pre-industrial levels of mercury in the teeth of *Beluga* in the Mackenyie Delta, Northwest Territories, and *Walrus* at Iglookik, Nunavut, Canada. *Arctic*, **55**, 123 (2002).
7. Johnson, K. P. *et al.* Investigation of the deposition and emission of mercury in arctic snow during an atmospheric mercury depletion event. *J. Geophys. Res.* **113**, D17, D17304 (2008).
8. NADP 2016. National Atmospheric Depostion Program, Annual Data, all MDN sites. http://nadp.sws.uiuc.edu/data/mdn/annual.aspx (Oct 3, 2016).
9. Schuster P. F. *et al.* Mercury export from the Yukon river basin and potential response to a changing climate. *Environ. Sci. Technol.* **45**, 9262-9267 (2011).

10. Fisher J. A. *et al.* Riverine source of Arctic Ocean mercury inferred from atmospheric observations. *Nat. Geosci.* **5**, 499-504 (2012).
11. Dastoor, A. P. & Durnford, D. A. Arctic Ocean: Is It a sink or a source of atmospheric mercury? *Environ. Sci. Technol.* **48**, 1707-1717 (2014).
12. Demers, J. D., Blum, J.D. & Zak, D. R. Mercury isotopes in a forested ecosystem: Implications for air-surface exchange dynamics and the global mercury cycle. *Global Biogeochem Cy.* **27**, 222-238 (2013).
13. Jiskra, M. *et al.* Mercury deposition and re-emission pathways in boreal forest soils investigated with Hg isotope signatures. *Environ. Sci. Technol.* **49**, 7188-7196 (2015).
14. Enrico, M. *et al.* Atmospheric mercury transfer to peat bogs dominated by gaseous elemental mercury dry deposition. *Environ. Sci. Technol.* **50**, 2405-2412 (2016).
15. Zheng, W., Obrist, D., Weis, D., & Bergquist, B. A. Mercury isotope compositions across North American forests. *Global Biogeochem Cy.* **30**, 1475-1492 (2016).
16. Krabbenhoft, D. & Sunderland, E.M. Global Change and Mercury. *Science* **341**, 1457-1458 (2013).
17. Polyakov IV, Alekseev GV, Bekryaev RV, Bhatt U, Colony RL, Johnson MA, et al. Observationally based assessment of polar amplification of global warming. *Geophys. Res. Letters* **29**, 1878 (2002).
18. ACIA, "Impacts of a warming Arctic: Arctic Climate Impact Assessment. ACIA Overview report" (Cambridge University Press, 2004).
19. Selin N.E, Global change and mercury cycling: challenges for implementing a global treaty. *Environmental Toxicology and Chemistry* **33**, 1202 (2014).
20. Smith-Downey, N. V., Sunderland, E. M. & Jacob, D. J. Anthropogenic impacts on global storage and emissions of mercury from terrestrial soils: Insights from a new global model. *J Geophys Res-Biogeo.* **115**, 11 (2010).
21. Steffen, A. *et al.* A synthesis of atmospheric mercury depletion event chemistry in the atmosphere and snow. *Atmos. Chem. Phys.* **8**, 1445-1482 (2008).
22. Agnan, Y. *et al*. New constraints on terrestrial surface-atmosphere fuxes of gaseous elemental mercury using a global database. *Environ. Sci. Technol.* **50**, 507-524 (2016).
23. Sherman L. S. *et al.* Mass-independent fractionation of mercury isotopes in Arctic snow driven by sunlight. *Nat. Geosci.* **3**, 173-177 (2010).
24. Biswas, A. *et al.* Natural mercury isotope variation in coal deposits and organic soils. *Environ. Sci. Technol.* **42**, 8303-8309 (2008).
25. Obrist, D., Pokharel, A. K. & Moore, C. Vertical profile measurements of soil air suggest immobilization of gaseous elemental mercury in mineral soil. *Environ. Sci. Technol.* **48**, 2242-2252 (2014).
26. Obrist et al. Mercury distribution across 14 U.S. Forests. Part I: spatial patterns of concentrations in biomass, litter, and soils. *Environ. Sci. Technol.* 45, 3974-3981 (2011).
27. Smith D.B. et al. Geochemical and mineralogical data for soils of the coterminous United States. *U.S. Geological Survey Data Series* **801**, 386p (2013).
28. Amos H. M. *et al.* Observational and modeling constraints on global anthropogenic enrichment of mercury. *Environ. Sci. Technol.* **49**, 4036-4047 (2015).
29. Hararuk, O., Obrist, D. & Luo, Y. Modelling the sensitivity of soil mercury storage to climate-induced changes in soil carbon pools. *Biogeosciences* **10**, 2393-2407 (2013).
30. Sprovieri F, *et al*. Atmospheric mercury concentrations observed at ground-based monitoring sites globally distributed in the framework of the GMOS network. *Atmos. Chem Phys.* **16**, 11915-11935. (2016).

Methods References

31. Fritsche, J. *et al.* Elemental mercury fluxes over a sub-alpine grassland determined with two micrometeorological methods. *Atmos. Environ.* **42**, 2922-2933 (2008).
32. Castro, M. & Moore, C. Importance of gaseous elemental mercury fluxes in western Maryland. *Atmosphere* **7**, 110 (2016).
33. Douglas, T. A. *et al.* Influence of snow and ice crystal formation and accumulation on mercury deposition to the Arctic. *Environ. Sci. Technol.* **42**, 1542-1551 (2008).
34. Cole, A.S. *et al*. Ten-year trands of atmospheric mercury in the high Arctic compared to Canadian sub-Arctic and mid-latitude sites. *Atmsph. Chem. Phys*. **13**, 1535 (2013).
35. Seok, B. *et al.* An automated system for continuous measurements of trace gas fluxes through snow: an evaluation of the gas diffusion method at a subalpine forest site, Niwot Ridge, Colorado. *Biogeochemistry* **95**, 95-113 (2009).
36. Faïn, X. *et al*. Mercury dynamics in the Rocky Mountain, Colorado, snowpack. *Biogeosciences* **10**, 3793-3807 (2013).
37. Moore, C. W., Obrist, D. & Luria, M. Atmospheric mercury depletion events at the Dead Sea: Spatial and temporal aspects. *Atmos. Environ.* **69**, 231-239 (2013).
38. Edwards, G. C. *et al.* Development and evaluation of a sampling system to determine gaseous mercury fluxes using an aerodynamic micrometeorological gradient method. *J. Geophy. Res.-Atmos.* **110**, (2005).
39. Lyman, S. N. & Jaffe, D. A. Formation and fate of oxidized mercury in the upper troposphere and lower stratosphere. *Nat Geosci* **5**, 114-117 (2012).
40. Zhang, L., Wright, L. P. & Blanchard, P. A review of current knowledge concerning dry deposition of atmospheric mercury. *Atmos. Environ.* **43**, 5853-5864 (2009).
41. Shaver, G. R., Chapin, F. S. Production: Biomass relationships and element cycling in contrasting Arctic vegetation types. *Ecol. Monogr.* **61**, 1-31 (1991).
42. Chapin, F. S., Shaver, G. R., Giblin, A. E., Nadelhoffer, K. J. & Laundre, J. A. Responses of Arctic tundra to experimental and observed changes in climate. *Ecology* **76**, 694-711 (1995).
43. Fu, X. , Heimburger, L.-E. & Sonke, J. E. Collection of atmospheric gaseous mercury for stable isotope analysis using iodine- and chlorine-impregnated activated carbon traps. *J. Anal. At. Spectrom.* **29**, 841-852 (2014).

Acknowledgements: We thank Toolik Field Station and Polar Field Services staff for their support in setting up field site and maintaining operation for two years, with special thanks to Jeb Timm. We thank Olivia Dillon and Christopher Pearson for support with laboratory analyses, Alexandra Steffen and Steve Brooks for providing additional instrumentation, as well as Roger Kreidberg and Jay Arnone for editorial and technical assistance in manuscript preparation. The Hg isotope work was funded by H2020 Marie Sklodowska-Curie grant agreement No 657195 to MJ and European Research Council grant ERC-2010-StG_20091028 and CNRS-INSU-CAF funding (PARCS project) to JES.

Author contributions: D.O. and D.H. designed and initiated the project, and M.J., J.S. and D.O. designed and developed the isotope component. All authors were involved in all major field sampling and/or laboratory analyses. Y.A. led data analysis and M.J. led stable isotope sampling and analysis with support by J.S. D.O. led manuscript writing with major support by M.J. Y.A. J.S. and C.M.

Additional information: Supplementary Information accompanies this paper at http://www.nature.com/

Competing financial interests: The authors declare no competing financial interests.

Data availability statement: Hg Concentration data in plants, soils, precipitation and snowpack generated during this study are included in the Extended Data section as Tables. Stable isotope data are also included in Extended Data and in Supplementary Information. Additional data (e.g., flux data) as well as higher-resolution datasets are available from the corresponding author on reasonable request.

484

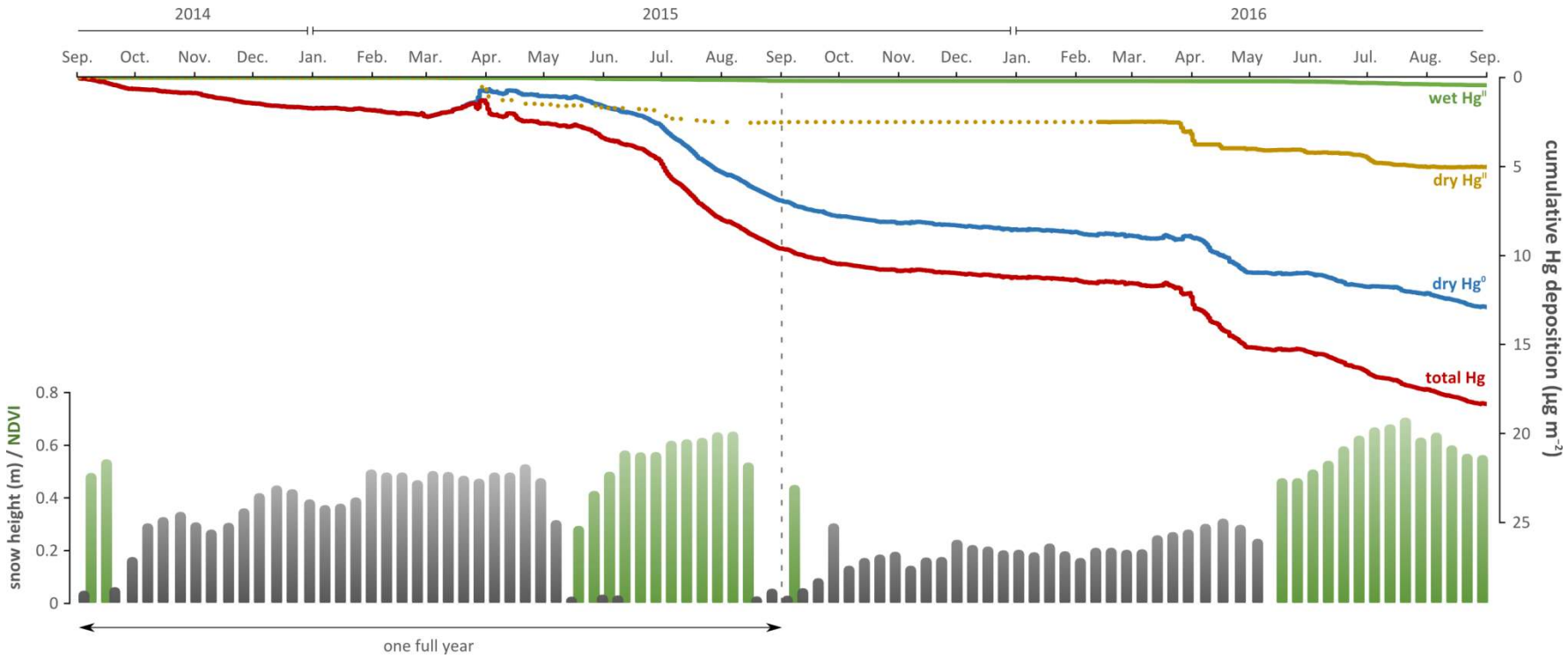

Figure 1. Cumulative atmospheric deposition of major Hg forms in the Arctic tundra. Blue line: gaseous Hg^0 flux; green line: wet Hg deposition (Hg^{II}) ; brown line: dry deposition of Hg^{II}; dashed line shows observations extrapolated when not measured. Bottom panel shows snow heights and vegetation coverage.

485

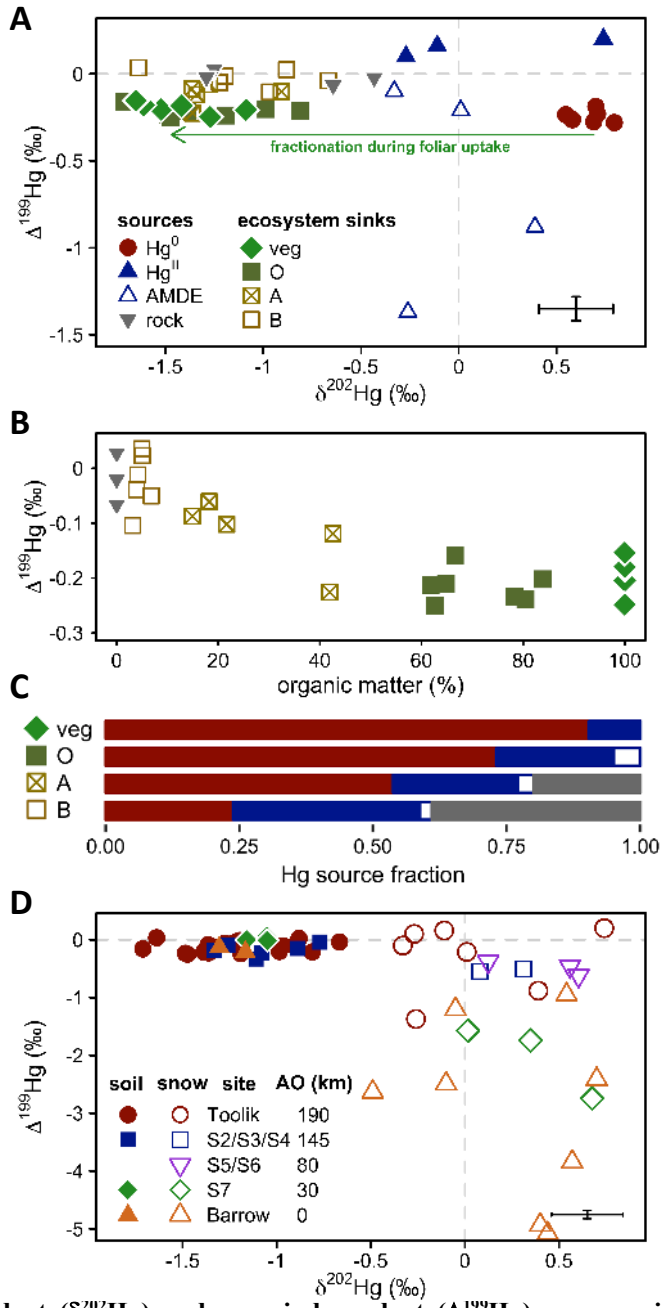

Figure 2 A. Mass-dependent (δ^{202}Hg) and mass-independent (Δ^{199}Hg) mercury isotope signatures in the tundra. Uncertainty (2 SD of replicate standards) shown on lower right. Symbols for sources include: filled circles for atmospheric Hg^0; filled triangles for Hg^{II} in snow deposited before Jan/Feb 2016; open triangles for Hg^{II} measured in surface snow during periods of AMDEs (Mar/Apr 2016); and filled inverted triangles for geogenic Hg in rock samples. Symbols for tundra samples include: filled diamonds for bulk vegetation; filled squares for organic (O-horizon) soils; and open squares for mineral soils (with cross for A horizons [>10% organic matter] and without cross for B horizons [<10% organic matter]). Arrow represents mass-dependent fractionation of atmospheric Hg^0 during foliar uptake. **B. Linear correlation of Δ^{199}Hg with organic matter content**, showing that signatures of terrestrial samples can be explained predominantly by binary mixing of the two endmembers geogenic Hg and vegetation Hg. **C. Fraction of respective Hg sources in vegetation and soils. D. δ^{202}Hg and Δ^{199}Hg mercury isotope signatures of soils (O, A, B horizons) and snow (collected during Mar/Apr) along an inland-to-coastal transect.** Distance from Arctic Ocean (AO) is given in km. Barrow samples are from [23,24].

486

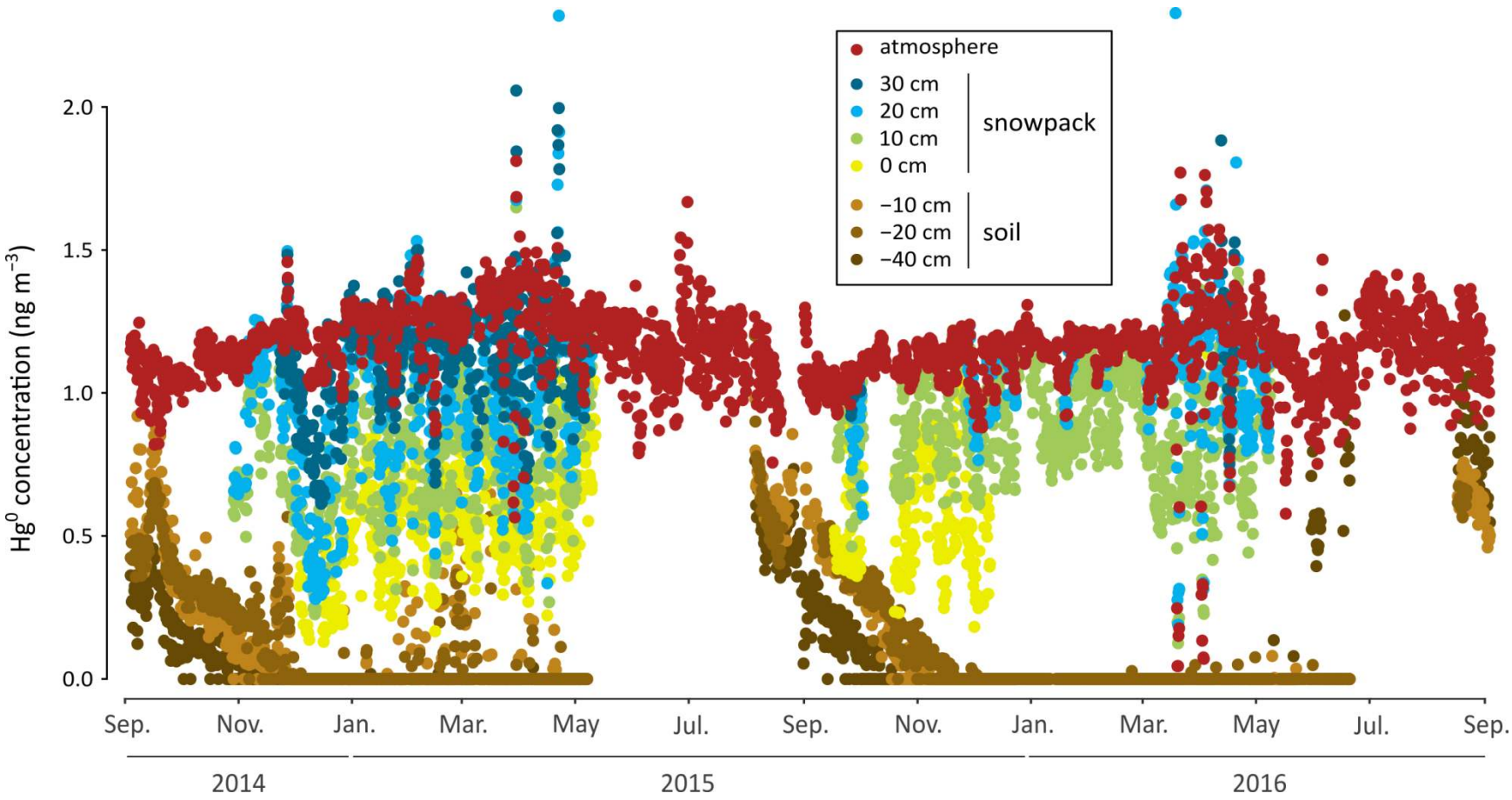

Figure 3. Gaseous Hg^0 concentrations in the atmosphere, interstitial snow air, and tundra soil pores. Zero-values in soils show concentration measurements below the detection limits. Different symbol colors represent different heights in snowpack and different depths in soils. Snowpack heights (in cm) show height in snowpack above the ground surface. Soil depth (in cm, negative numbers) show depth of measurements in soil pores below the ground surface.